Effective Methods to Correct Contrast Agent–Induced Errors in PET Quantification in Cardiac PET/CT

Florian Büther*[1], Lars Stegger[1], Mohammad Dawood[1], Felix Range[2], Michael Schäfers[1], Roman Fischbach[3], Thomas Wichter[2], Otmar Schober[1], and Klaus P Schäfers*[1]

[1]Department of Nuclear Medicine, University of Münster, Münster, Germany; [2]Department of Cardiology and Angiology, University of Münster, Münster, Germany; and [3]Department of Clinical Radiology, University of Münster, Münster, Germany

In combined PET/CT studies, x-ray attenuation information from the CT scan is generally used for PET attenuation correction. Iodine-containing contrast agents may induce artifacts in the CT-generated attenuation map and lead to an erroneous radioactivity distribution on the corrected PET images. This study evaluated 2 methods of thresholding the CT data to correct these contrast agent–related artifacts. **Methods:** PET emission and attenuation data (acquired with and without a contrast agent) were simulated using a cardiac torso software phantom and were obtained from patients. Seven patients with known coronary artery disease underwent 2 electrocardiography-gated CT scans of the heart, the first without a contrast agent and the second with intravenous injection of an iodine-containing contrast agent. A 20-min PET scan (single bed position) covering the same axial range as the CT scans was then obtained 1 h after intravenous injection of ^{18}F-FDG. For both the simulated data and the patient data, the unenhanced and contrast-enhanced attenuation datasets were used for attenuation correction of the PET data. Additionally, 2 threshold methods (one requiring user interaction) aimed at compensating for the effect of the contrast agent were applied to the contrast-enhanced attenuation data before PET attenuation correction. All PET images were compared by quantitative analysis. **Results:** Regional radioactivity values in the heart were overestimated when the contrast-enhanced data were used for attenuation correction. For patients, the mean decrease in the left ventricular wall was 23%. Use of either of the proposed compensation methods reduced the quantification error to less than 5%. The required time for postprocessing was minimal for the user-independent method. **Conclusion:** The use of contrast-enhanced CT images for attenuation correction in cardiac PET/CT significantly impairs PET quantification of tracer uptake. The proposed CT correction methods markedly reduced these artifacts; additionally, the user-independent method was time-efficient.

Both PET and CT can provide valuable diagnostic and prognostic information noninvasively to guide the management of patients with heart disease. Molecular and functional PET can be used, for example, to assess myocardial perfusion, perfusion reserve, metabolism, and innervation. With morphologic CT, calcification of coronary arteries may be detected and quantified, and modern equipment even allows for the noninvasive visualization of the vessel lumen (coronary angiography). The main advantage of combined PET/CT devices over stand-alone PET and CT lies in the acquisition of both molecular and morphologic data with spatial and temporal coregistration in a single session, making data interpretation easier and quicker. It is self-evident that the PET/CT protocol has to be tailored to each patient to minimize radiation exposure and scanning time. Unnecessary scans have to be avoided. Unlike stand-alone PET scanners, attenuation correction of the PET data in PET/CT studies is usually not based on a separate PET transmission scan using external rod sources. Instead, x-ray attenuation information from the CT scan is used to derive the PET attenuation map—a method that is faster and provides attenuation maps that are less noisy. However, this approach may also be a source of new image artifacts and may bias quantification of tracer uptake. Artifacts may be introduced by motion because of the different timescales of CT and PET data acquisition, potentially leading to spatial nonconformance of the CT and PET data (*1*). This problem is especially prominent in cardiac PET/CT, because respiratory and cardiac motion causes the heart to move during the PET scan, whereas CT scans are usually acquired during a breath-hold and corrected for cardiac motion by prospective electrocardiography triggering. Different strategies are currently being developed worldwide to correct for these motion-induced artifacts.

Additional artifacts may be introduced when contrast-enhanced CT data, such as that acquired during CT-based coronary angiography, are used for PET attenuation correction. The use of these data instead of a separate unenhanced CT acquisition can reduce radiation exposure to the patient and decrease scanning time. This approach may therefore be worthwhile provided that PET image quality remains adequate and that necessary postprocessing is feasible in a clinical setting.

Standard CT-to-PET attenuation transformations work well for body tissues such as soft tissue and bones; however, they fail to compute the appropriate attenuation values in the presence of iodine, because iodine absorbs 511-keV photons similarly to soft tissue but is an extremely effective absorber at CT energies (2). The result is an overestimation of absorption values for PET attenuation correction and thereby wrong quantification of radioactivity by PET.

The question of whether oral or intravenous CT contrast agents have a clinically relevant impact on the evaluation of PET images has been discussed before, but mainly with regard to whole-body tumor imaging. The results of most studies imply that contrast-enhanced CT data can indeed be used for attenuation correction in most tumor-staging studies. However, the impact of contrast agents in PET/CT of the heart has not yet been fully evaluated (3). The aim of this study was therefore to evaluate the effect of using contrast-enhanced CT data for PET attenuation correction in cardiac PET/CT and to develop and validate sufficient correction methods. To this aim, both a software phantom and data from a patient study were used.

MATERIALS AND METHODS

PET/CT Scanner

PET and CT data were acquired on a Biograph Sensation 16 PET/CT scanner (Siemens Medical Solutions) equipped with PET list-mode acquisition software. The CT scanner was equipped with an integrated electrocardiography device and could be run with tube currents of 28–500 mA. The possible tube voltage settings were 80, 120, and 140 kV. The transaxial field of view (FOV) was 500 mm.

The PET scanner comprised 24 detector rings (ring diameter, 827 mm) with 384 lutetium oxyorthosilicate detectors each, resulting in a total of 9,216 detectors. The axial FOV was 162 mm, and the transaxial FOV was 585 mm. The list-mode software allowed recording of coincidence events together with time information to a list-mode file that could be processed retrospectively.

Software Phantom Data

The nonuniform rational B-splines–based cardiac-torso (NCAT) software phantom (4) was applied to simulate the effects of using contrast-enhanced CT data for attenuation correction in cardiac PET/CT. The phantom was developed to provide a realistic model of the human anatomy (Fig. 1). PET tracer activities and PET attenuation values could be attributed independently to every organ. For our study, 2 different attenuation maps were created: one simulating unenhanced CT data and another simulating contrast-enhanced CT information, both based on the corresponding mean attenuation values obtained from the patient scans. Sinogram raw data of PET emission were obtained by forward projection of phantom data using the open-source software package STIR (http://stir.hammersmithimanet.com).

The applied PET attenuation values were 0.093 and 0.094 cm^{-1} for body, 0.027 and 0.031 cm^{-1} for lung, 0.110 and 0.110 cm^{-1} for spine bone, 0.131 and 0.131 cm^{-1} for rib bone, 0.098 and 0.118 cm^{-1} for blood, 0.097 and 0.105 cm^{-1} for heart, and 0.098 and 0.103 cm^{-1} for liver, where the first value refers to unenhanced attenuation and the second is the contrast-enhanced value. The assigned PET tracer activities were 4 kBq/mL for body, 2 kBq/mL for lung, 2 kBq/mL for spine bone, 2 kBq/mL for rib bone, 4 kBq/mL for blood, 35 kBq/mL for heart, and 10 kBq/mL for liver.

Patient Data and Preparation

Seven patients with known coronary heart disease were included in this study. Patients were routinely referred for ^{18}F-FDG PET for evaluation of myocardial viability before revascularization. Ninety minutes before scanning, the patients received an oral β-blocker to slow the heart rate. A hyperinsulinemic euglycemic clamp was applied before and during the scans to enhance ^{18}F-FDG uptake in the heart (5). For the PET scan, the patients received an intravenous dose of 4 MBq of ^{18}F-FDG per kilogram of body weight 60 min before PET scanning began.

Data Acquisition

During the PET/CT scan, the patients were positioned supine with the arms elevated behind the head. First, a CT topogram of the thorax was obtained to position the heart in the FOV of the PET/CT scanner. Next, an unenhanced CT scan with retrospective electrocardiography gating was initiated (calcium scoring protocol, 120-kVp tube voltage, 133-mAs effective tube current, 16 × 0.75 mm collimation, 420-ms rotation time, pitch of 0.46, 12-s scanning time) and was used as reference data for PET attenuation correction (Fig. 2A). Another electrocardiography-gated, contrast-enhanced CT scan for visualization of the coronary arteries (120-kVp tube voltage, 550-mAs effective tube current, 16 × 0.75 mm collimation, 420-ms rotation time, pitch of 0.28, 20-s scan time) was then obtained for all patients during intravenous injection of a bolus of iodine-containing contrast agent (Ultravist 370 [Schering],

FIGURE 1. From left to right, transversal, coronal, and sagittal views of NCAT software phantom. Specific PET activities and attenuation values can be assigned to every organ inside torso.
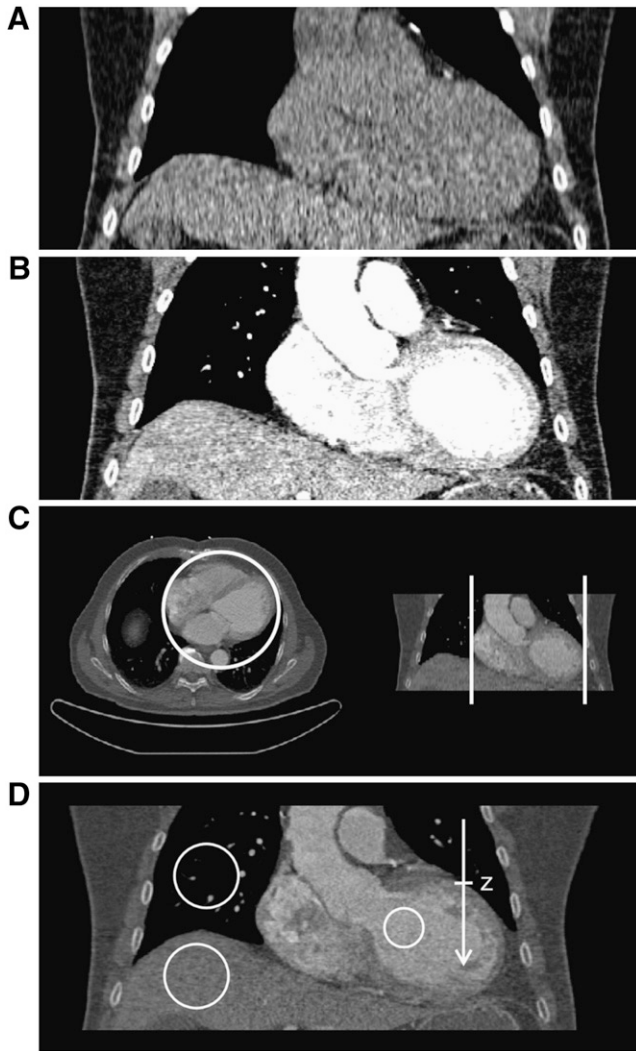
FIGURE 2. CT images of heart: (A) Unenhanced CT scan, coronal view, soft-tissue window (center, 50 HU; width, 350 HU). (B) Contrast-enhanced CT scan, coronal view, soft-tissue window. Influence of contrast agent is clearly visible (attenuation value in left ventricle, 370 HU; reference value, 30–45 HU). (C) Cylinder-based CT segmentation of contrast agent in heart area, with transversal view on left and coronal view on right. Every CT pixel value above normal tissue value inside cylinder is considered to represent contrast agent and reduced to 35 HU (cylinder-threshold correction). (D) Size and location of ROI used to determine mean attenuation and uptake values in CT and PET images, respectively (Tables 1 and 2). Also shown is position of heart–lung borderline along craniocaudal axis. Difference in craniocaudal position in the 2 CT images (unenhanced and enhanced) serves as measure of respiratory motion shift of heart.

140 mL, flow of 4 mL/s, followed by a saline chaser bolus) (Fig. 2B). The scan delay was determined using software that automatically detects the bolus (CARE Bolus; Siemens Medical Solutions), with a threshold of 100 Hounsfield units (HU). The patients were told to hold their breath in mid inspiration during the CT scans. Directly after the contrast-enhanced CT scan, a 20-min list-mode PET scan was acquired. The resulting PET list-mode file contained information on both coincidence and timing data.

Data Reconstruction

Raw CT datasets acquired in end-diastole at 90% of the R-R interval were used for PET attenuation correction. CT images were reconstructed using the standard manufacturer-supplied software for both the unenhanced CT scan (110 slices, 512×512 matrix, 500-mm FOV, 0.977-mm pixels, 3-mm-thick slices, 1.5-mm increment, 165-mm axial scan range) and the enhanced CT scan (330 slices, 512×512 matrix, 500-mm FOV, 0.977-mm pixels, 1-mm-thick slices, 0.5-mm increment, 165-mm axial scan range). The CT images were resized to match the PET matrix size ($175 \times 175 \times 47$) and resolution (3.375-mm voxel length), and a Gaussian filter was applied to match the PET resolution. Because the CT images contained attenuation information for effective photon energies of about 70 keV, given in HU, they had to be transformed to PET photon energies of 511 keV (μ-maps). For this purpose, different approaches have been developed and implemented in commercially available tomographs (*2*). In this study, we used the following established bilinear algorithm (*6*):

$$\mu^{PET}(CT \leq 0\,HU) = \mu^{PET}_{H_2O}(CT + 1,000)/1,000$$

$$\mu^{PET}(CT > 0\,HU) = \mu^{PET}_{H_2O} + CT\frac{\mu^{PET}_{H_2O}(\mu^{PET}_{Bone} - \mu^{PET}_{H_2O})}{1,000(\mu^{CT}_{Bone} - \mu^{CT}_{H_2O})},$$

where CT denotes the CT image value in HU and the different μ values represent the linear absorption coefficients of bones and water at CT and PET energies, respectively. The following values were used:

$$\mu^{PET}_{H_2O} = 0.096\,cm^{-1}$$

$$\mu^{PET}_{Bone} = 0.172\,cm^{-1}$$

$$\mu^{CT}_{H_2O} = 0.184\,cm^{-1}$$

$$\mu^{CT}_{Bone} = 0.428\,cm^{-1}.$$

Both attenuation maps (unenhanced CT and enhanced CT) were used for PET attenuation correction. Two additional attenuation maps were derived from the enhanced CT datasets using 2 methods of reducing interference from contrast enhancement.

In the first method, every CT pixel value above 35 HU inside an axially aligned cylindric region of interest (ROI) tightly enclosing the

TABLE 1
CT Attenuation Averaged Over All 7 Patients in Organs Measured in Spheric ROIs*, with Corresponding Uptake

CT method	CT attenuation in ROI (HU)			Uptake in ROI (%)		
	Heart	Lung	Liver	Heart	Lung	Liver
Unenhanced	43	−805	57	100	100	100
Enhanced	354	−744	92	146	124	113

*Of 25-mm diameter inside left ventricle and 40-mm diameter inside right lung and liver.
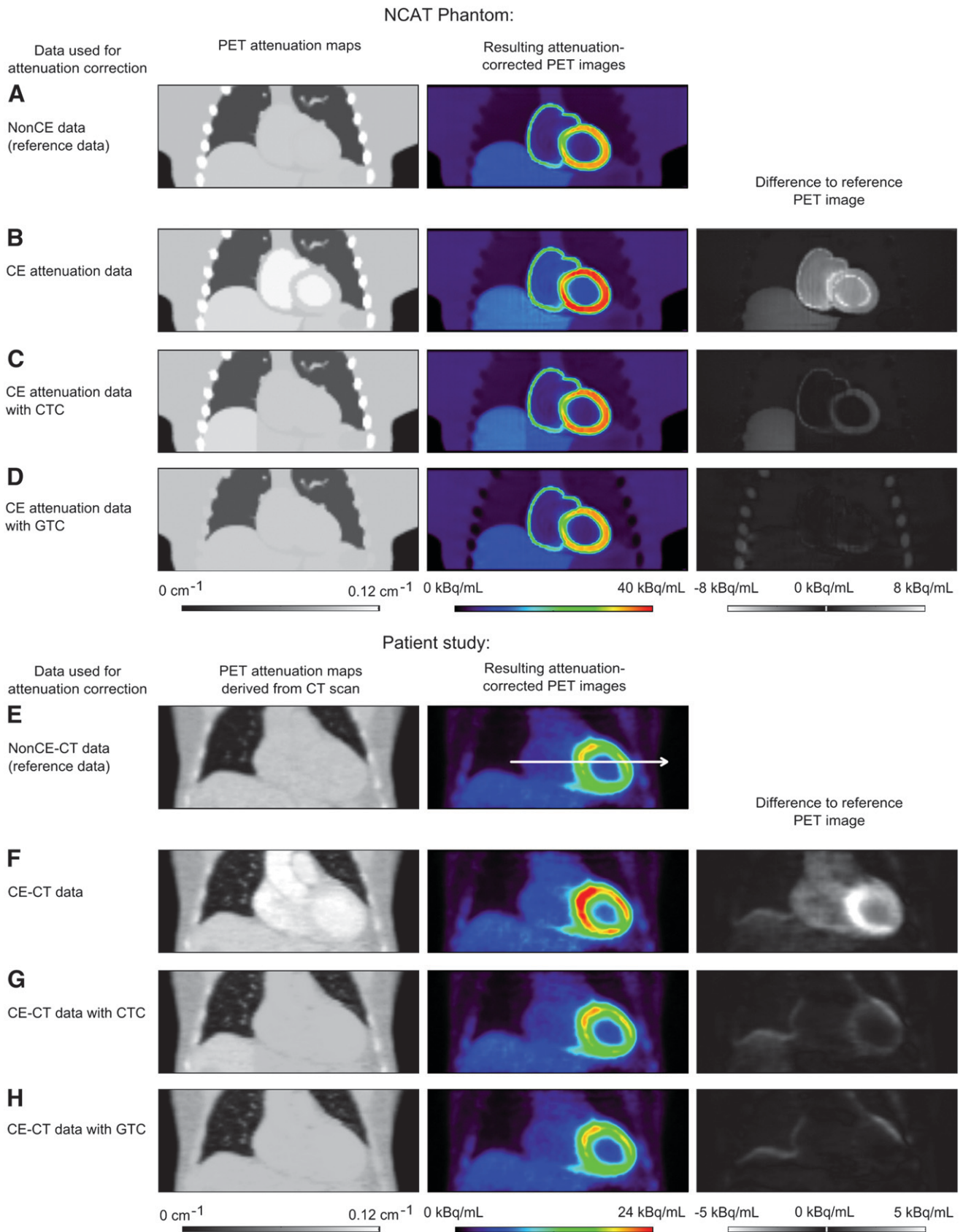
FIGURE 3. PET attenuation maps and corresponding attenuation-corrected PET images of NCAT phantom (A–D) and typical patient scan (E–H), based on the following attenuation data: unenhanced data (reference data; mean CT attenuation in left ventricle in E, 40 HU) (A and E); nonprocessed contrast-enhanced data (mean CT attenuation in left ventricle in F, 370 HU) (B and F);

heart but excluding the thoracic bones (Fig. 2C) was set to 35 HU, a typical value for normal, unenhanced soft-tissue attenuation (cylinder-threshold correction). This cylindric region was defined interactively by the operator. Use of this method is motivated by the high concentrations of contrast agent confined to the heart cavities alone. In the second method, this threshold technique was expanded to the entire FOV, thus additionally reducing the attenuation coefficients attributed to extracardiac accumulations of contrast agent and, as a side effect, high-density structures such as bone (global-threshold correction). This expansion was done to additionally account for widespread low concentrations of contrast agent in the body. For simulated data from the NCAT phantom, a threshold of 0.097 cm^{-1}, corresponding to the CT threshold of 35 HU, was chosen. Four different attenuation maps (resulting in 4 different attenuation-corrected PET image sets) were thus generated for the simulated phantom data and for every patient.

The PET list-mode file (typically around 1.5 GB of PET coincidence raw data) was binned into sinogram datasets using software developed in-house specifically for this purpose. Corrections for decay, dead time, detector normalization, calibration, and scatter (convolution-subtraction algorithm) were applied to the sinograms (7).

The preprocessed sinogram sets were reconstructed using STIR with an iterative 3-dimensional ordered-subsets expectation maximization algorithm to obtain the PET images. The reconstruction included 4 subsets and 5 iterations. The obtained images comprised $175 \times 175 \times 47$ cubic voxels with an edge length of 3.375 mm.

Data Analysis

ROIs were analyzed for the 4 CT and 4 attenuation-corrected PET images to investigate the influence of contrast agents on CT and PET quantification. Three representative locations were chosen: inside the left ventricular cavity near the valve plane (25-mm-diameter spheric ROI; Fig. 2D) and the right lung and the liver (40-mm-diameter spheric ROIs; Fig. 2D). Mean CT attenuation and PET tracer uptake were determined. The ratio of uptake using the original CT data and the 2 sets of corrected enhanced CT data to uptake using the unenhanced CT data was obtained as a measure of the impact of contrast agent and contrast agent correction. Additionally, regional uptake for 384 myocardial segments was measured using an automated 3-dimensional segmentation algorithm described elsewhere (8,9). In brief, the left ventricle was aligned along its long axis, and image data were transformed using a cylindric coordinate system for the basal and midventricular ventricle and a spheric coordinate system for the apical portion (bottle brush approach). Endo- and epicardial contours were derived by an algorithm based on a physical model of an elastic membrane in a field of force. Spatial sampling (16 steps from base to apex; 24 steps in the azimuth direction) and the endo- and epicardial contours defined 384 approximately wedge-shaped segments in the left ventricular myocardium. The maximum value within each myocardial segment was displayed in a polar map to derive regional myocardial uptake. Linear correlation plots of uptake per polar map segment were drawn using the enhanced CT
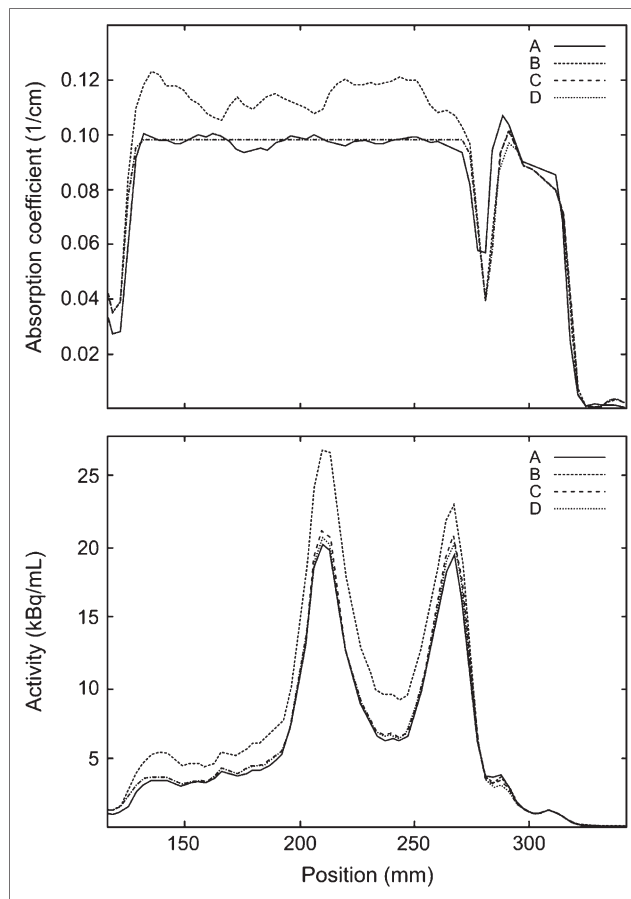
FIGURE 4. Attenuation map (top) and PET (bottom) line profiles through heart (Fig. 3E), with attenuation data from unenhanced CT scan (A), nonprocessed contrast-enhanced CT scan (B), contrast-enhanced CT scan with cylinder-threshold contrast agent correction (C), and contrast-enhanced CT scan with global-threshold contrast agent correction (D).

data in relation to the unenhanced CT data. The slope of linear fit served as another measure of the impact of contrast agent and contrast agent correction.

For patients, the enhanced CT data and the unenhanced CT data were acquired during separate scans. Therefore, a difference in breath-hold positions may have been a confounding factor in this study, but it was the effect of contrast agent—and not the effect of respiratory motion—that was at the center of this work. The degree of mismatch between the enhanced and unenhanced CT scans was deduced by placing a craniocaudal axial line profile through the center of a left ventricular coronal slice on both scans (Fig. 2D). The difference in axial positioning of the borderline between heart and lung tissue approximated the shift of the heart due to respiratory motion.

FIGURE 3. (Continued)
contrast-enhanced data with cylinder-threshold contrast agent correction (C and G); and contrast-enhanced data with global-threshold contrast agent correction (D and H). Shown on right are differences between PET images based on CE attenuation data and PET images based on unenhanced CE data. PET images using nonprocessed enhanced CT scan information overestimate uptake in left ventricular wall. Arrow in E refers to line profile of Figure 4. CE = contrast-enhanced; CTC = cylinder-threshold correction; GTC = global threshold correction.

TABLE 2
Uptake in Spheric ROI* Inside Left Ventricle, as Measured in NCAT Phantom and Patients

| | Uptake in ROI (%) | | |
| | | Patients | |
Source of attenuation data	NCAT phantom, mean	Mean	Range
CE data, nonprocessed	166	146	131–159
CE data, cylinder-threshold correction	101	104	102–107
CE data, global-threshold correction	99	102	100–103

*Of 25-mm diameter.
Images obtained with unenhanced CE attenuation data were used as reference value (100%).

RESULTS

ROI analysis of the CT images revealed the impact of using contrast agents in cardiac CT (Table 1). On average, the left ventricular CT attenuation value increased from approximately 40 HU (unenhanced CT; range, 38–53 HU) to 350 HU (enhanced CT; range, 264–424 HU). However, this influence was not confined to the interior of the heart, as demonstrated by the increased ROI values of the right lung and liver, indicating significant contrast agent widespread in the body. This increase in CT attenuation correspondingly increased PET uptake values, which were highest in the heart (46%), followed by the lung (24%) and the liver (13%).

Figure 3 demonstrates the NCAT phantom study and a typical patient study. The difference images (Figs. 3B–3D and 3F–3H) show the discrepancy from using enhanced and unenhanced data for PET attenuation correction. Additionally, these images demonstrate that both contrast agent correction methods effectively removed the influence of the agent on the PET images. When used on unenhanced CT data, the simple global-threshold method (Figs. 3D and 3H) gave uptake results in the heart almost identical to those from the PET data, as was also verified for the patient scan by a PET line profile through the heart (Fig. 4).

Analysis of mean uptake in a spheric ROI inside the left ventricle revealed that radioactivity was overestimated for all patients and for the NCAT phantom when attenuation was corrected using enhanced CT data (patients, 131%–159%; NCAT phantom, 166%), compared with unenhanced CT data (Table 2). This influence was effectively reduced using the contrast agent–corrected CT data; global-threshold correction worked best (100%–103% and 99% for the patients and the NCAT phantom, respectively).

Similar behavior was seen in polar map analysis of the left ventricle (Fig. 5). The slope of the linear fit in correlation plots (Fig. 6) was considered mean uptake in the left ventricular wall relative to uptake using unenhanced data and depended directly on the influence of contrast agent on PET attenuation correction in the heart. In the presented patient scan, the slope was 1.230, showing that mean uptake in the left ventricular wall was overestimated by 23%. Using the correction methods, the slope decreased to 1.048 (cylinder-

threshold correction) and 1.017 (global-threshold correction), which are similar to the ideal value, 1. The averaged slopes for the NCAT phantom, all patients, and all methods are shown in Table 3. In general, polar maps from PET images that were attenuation-corrected using nonprocessed contrast-enhanced data resulted in increased uptake in the left ventricular wall (23% on average), whereas corrected PET images led to a more consistent quantification (8% and 4% increases for the cylinder-threshold and global-threshold corrections, respectively).

The correlation between relative mean uptake in the left ventricular wall and the respiratory motion shift between
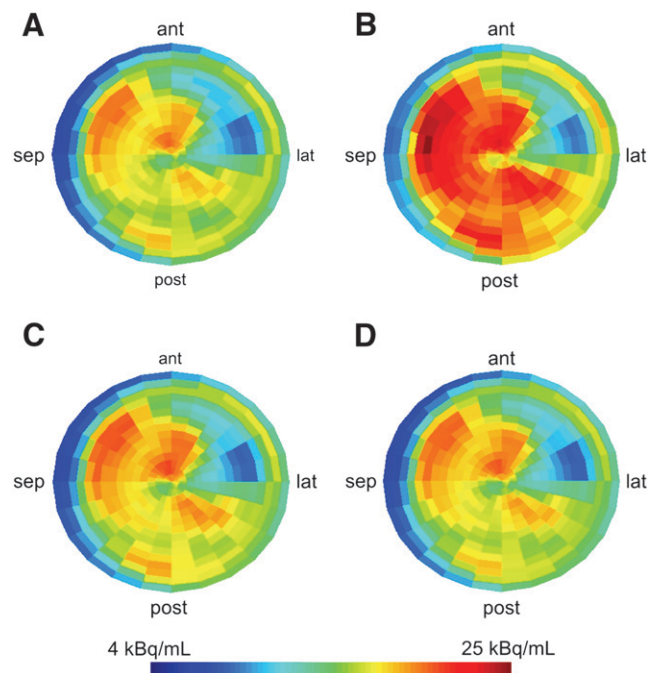
FIGURE 5. Polar maps of patient scans of Figure 3 using attenuation data from unenhanced CT scan (A), nonprocessed contrast-enhanced CT scan (B), contrast-enhanced CT scan with cylinder-threshold correction (C), and contrast-enhanced CT scan with global-threshold correction (D). Uptake in left ventricle is overestimated when using nonprocessed contrast-enhanced CT attenuation data. ant = anterior; lat = lateral; post = posterior; sep = septal.
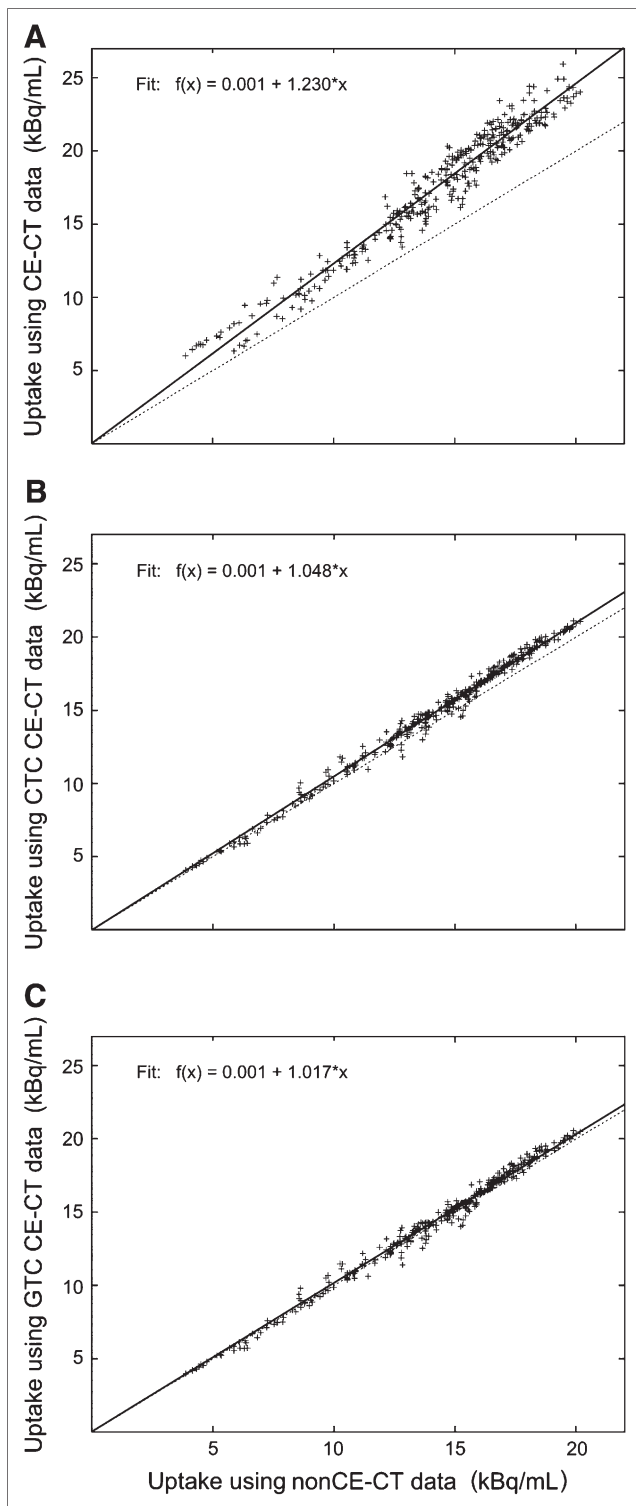
FIGURE 6. Correlation of polar map segments of left ventricle using original (A) and corrected (B and C) contrast-enhanced CT attenuation data. Corrected attenuation data provide more reliable quantification. CE = contrast-enhanced; CTC = cylinder-threshold correction; GTC = global threshold correction.

the 2 CT scans revealed an additional influence from differences in respiration phase during the CT scans (Fig. 7). A linear relationship was well supported, with a correlation

coefficient of 0.943. The fit function was $f(x) = 0.015x + 0.995$.

DISCUSSION

Combined acquisition of molecular and morphologic parameters with PET/CT has the potential to optimize noninvasive cardiac imaging. For many patients, a scanning protocol that combines PET with CT-based coronary angiography will provide optimal diagnostic and prognostic information. The use of contrast-enhanced CT images, instead of a separate unenhanced CT scan, for PET attenuation correction would minimize radiation exposure to the patient and reduce scanning time. This study has shown, however, that the presence of a contrast agent can seriously impair the quality of PET attenuation correction. Quantification of uptake is inexact if this contrast agent–induced effect is not corrected. Our study confirmed the findings of Mawlawi et al. (*10*) that the use of "contrast agent–contaminated" CT for PET attenuation correction overestimates myocardial uptake on PET. The averaged mean signal increase in the left ventricular wall in our study was 23%, with a maximum of 44% in one patient, when compared with the values obtained from PET data attenuation-corrected by unenhanced CT data. This signal increase conflicts with the unique ability of PET to allow absolute quantification of radioactivity in vivo. It is clear that dependent on cardiac output and blood circulation times, the concentration of contrast agent—especially in the right ventricular cavity and other vascular structures during CT acquisition—can vary from patient to patient and that PET overestimation cannot be expected to be homogeneous. Not only quantitative analysis but also visual analysis of PET data may be adversely affected. In oncologic PET/CT, the use of intravenous enhanced CT data for attenuation correction has been found to produce image artifacts when the bolus injection results in high concentrations of contrast agent (*11,12*). However, other studies suggest that for tumor staging, this biased quantification usually does not change the diagnostic decision (*13–17*), especially if non–attenuation-corrected images are read alongside. This type of artifact can also be observed in cardiac PET/CT, especially in the region of the superior and inferior cava veins (*3*), and is likely to be more pronounced because CT coronary angiography requires data acquisition during an early arterial phase when the concentration of contrast agent in the blood is high, whereas oncologic CT is often acquired during the venous phase, when blood concentrations are lower. It seems unlikely that many physicians will tolerate this error for clinical cardiac imaging, because ambiguities are difficult to remove even when the non–attenuation-corrected data are alongside. One might conclude that unenhanced CT should be included in the scanning examination.

This study, however, has also shown that the 2 proposed correction algorithms can greatly alleviate this problem. The remaining error was slight in the phantom data and in the small patient cohort. One method proposed by

TABLE 3
Slope in Correlation Plots from Polar Maps of NCAT Phantom and Patients

		Patients	
Source of attenuation data	NCAT phantom	Mean	Range
CE data, nonprocessed	1.103	1.234	1.127–1.442
CE data, cylinder-threshold correction	1.038	1.084	1.018–1.213
CE data, global-threshold correction	0.994	1.044	0.977–1.169

*Relative mean uptake in left ventricular wall.

Nehmeh et al. (*18*) modifies the CT-to-PET transformation to account for massive concentrations of oral, barium-containing contrast agents in PET/CT of the abdomen and pelvis. In this study, we proposed another approach by using 2 clinically applicable threshold-based CT correction methods for cardiac PET/CT (cylinder-threshold correction and global-threshold correction). The study showed that the global-threshold method, especially, was simple to apply and produced satisfying results.

The main difficulty in determining the quality of correction methods in patient scans is the difference in respiratory phase between the 2 CT scans. This effect is demonstrated in the difference images in Figure 3, typically leading to a discrepancy in uptake in the anterolateral myocardial region and thus potentially interfering with correction for the contrast agent. The influence of respiration was investigated by correlating the axial shift of the heart in the 2 CT datasets to the residual uptake difference in the left ventricular wall after global-threshold correction (Fig. 7).
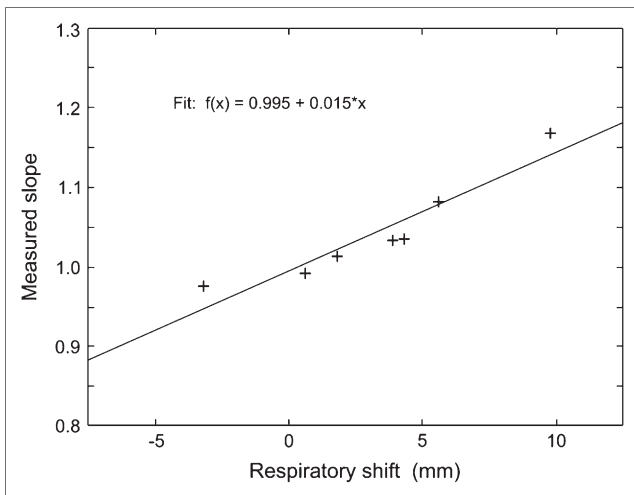
FIGURE 7. Correlation of mean uptake in left ventricle relative to reference CT data corrected using global-threshold correction (Table 3) and respiratory motion shift of left ventricle. Determined correlation coefficient is 0.943; *y*-axis intercept is 0.995.

Because a good correlation was found (correlation coefficient, 0.943), we assume that most of the residual uptake difference was not due to an insufficient correction for contrast agent but to respiratory differences. Further confirmation was given by the linear fit function f(x), which had a *y*-axis intercept ($x = 0$) of 0.995; therefore, identical respiratory phases during the 2 CT scans should result in virtually the same mean uptake when using the threshold-only correction method. Thus, it is safe to assume that global-threshold correction works even better than indicated by the averaged mean uptake of 104% (Table 3). This assumption is further supported by the ROI analysis of the cavity of the left ventricle (Table 2), which is less susceptible to differences in breathing phases because it is not as close to the heart–lung borderline as are parts of the left ventricular wall. The results of the NCAT phantom study (Table 3) further prove the effectiveness of the correction methods.

The fact that cylinder-threshold correction did not perform as well as global-threshold correction in the phantom and patient studies might be attributable to the low but widespread concentration of contrast agent outside the heart during enhanced CT. Of special interest in this context are the lung and the liver, because both lie close to the heart and contain a significant amount of blood. Values exceeding 35 HU are ignored in the cylinder-threshold correction method but are corrected in the global method. In the lungs, partial-volume effects may still lead to contrast-enhanced areas below 35 HU that are not corrected by either method. Indeed, an ROI analysis of the lungs (Table 1) demonstrated this increase: Averaged mean x-ray absorption was −805 HU on unenhanced CT and −744 HU on contrast-enhanced CT, leading to PET attenuation values of 0.019 cm^{-1} and 0.025 cm^{-1}, respectively. Similarly, attenuation in the liver was significantly increased but largely not corrected for in the cylinder-threshold method. This overestimation of PET attenuation even in cases of contrast agent correction was partly counterbalanced by the underestimation of attenuation in bone for global-threshold correction. In this small patient cohort, this approach leads to a remarkable similarity between PET values corrected by enhanced CT data and PET values corrected by unenhanced

CT data, although the effects of contrast agent are not completely removed in every pixel. A more sophisticated pixelwise correction would require segmentation of all organs and vessels, an overly complex task.

In this study, we used a published bilinear method to translate attenuation at CT photon energies to 511-keV annihilation photons. Another approach, the "hybrid" method described by Kinahan et al. (2), is based on a threshold of 300 HU instead of 0 HU to differentiate bone from nonbone regions, in addition to a different scaling factor for bone structures. We assured ourselves that both methods yield almost the same results; in particular, the conclusions drawn from the results for contrast agent corrections were independent of the applied method.

Studies on larger groups of patients are needed to show whether the use of contrast-enhanced CT images with global threshold correction is viable for routine imaging or whether other strategies, such as acquisition of a separate low-dose CT scan for PET attenuation correction, will provide more reliable data albeit with a higher total radiation dose. Another important factor in comparing the various possibilities is compatibility with motion correction algorithms, which remove another of the big obstacles in cardiac PET/CT.

CONCLUSION

The use of contrast-enhanced CT images for attenuation correction significantly overestimates myocardial uptake on PET. Global-threshold correction of CT attenuation values is a robust and fast method that significantly reduces this artifact.

ACKNOWLEDGMENTS

REFERENCES

1. Lang N, Dawood M, Büther F, Schober O, Schäfers M, Schäfers K. Organ movement reduction in PET/CT using dual-gated listmode acquisition. *Z Med Phys.* 2006;16:93–100.
2. Kinahan PE, Hasegawa BH, Beyer T. X-ray-based attenuation correction for positron emission tomography/computed tomography scanners. *Semin Nucl Med.* 2003;33:166–179.
3. Büther F, Schäfers KP, Stegger L, et al. Artifacts caused by contrast agents and patient movement in cardiac PET/CT. *Nuklearmedizin.* 2006;45:N53–N54.
4. Segars WP. *Development of a New Dynamic NURBS-Based Cardiac-Torso (NCAT) Phantom* [dissertation]. Chapel Hill, NC: University of North Carolina; 2001. Available at: www.bme.unc.edu/~wsegars/segars_NCAT_dis.pdf. Accessed May 7, 2007.
5. DeFronzo RA, Tobin JD, Andres R. Glucose clamp technique: a method for quantifying insulin secretion and resistance. *Am J Physiol.* 1979;237:E214–E223.
6. Burger C, Goerres G, Schoenes S, Buck A, Lonn AHR, von Schulthess GK. PET attenuation coefficients from CT images: experimental evaluation of the transformation of CT into PET 511 keV attenuation coefficients. *Eur J Nucl Med Mol Imaging.* 2002;29:922–927.
7. Bailey DL, Meikle SR. A convolution-subtraction scatter correction method for 3D PET. *Phys Med Biol.* 1994;39:411–424.
8. Stegger L, Hoffmeier AN, Schäfers KP, et al. Accurate noninvasive measurement of infarct size in mice with high-resolution PET. *J Nucl Med.* 2006;47:1837–1844.
9. Stegger L, Lipke CS, Kies P, et al. Quantification of left ventricular volumes and ejection fraction from gated ^{99m}Tc-MIBI SPECT: validation of an elastic surface model approach in comparison to cardiac magnetic resonance imaging, 4D-MSPECT and QGS. *Eur J Nucl Med Mol Imaging.* January 10, 2007 [Epub ahead of print].
10. Mawlawi O, Erasmus JJ, Munden RF, et al. Quantifying the effect of IV contrast media on integrated PET/CT: clinical evaluation. *AJR.* 2006;186:308–319.
11. Antoch G, Freudenberg LS, Egelhof T, et al. Focal tracer uptake: a potential artifact in contrast-enhanced dual-modality PET/CT scans. *J Nucl Med.* 2002;43:1339–1342.
12. Antoch G, Jentzen W, Freudenberg LS, et al. Effects of oral contrast agents on computed tomography-based positron emission attenuation correction in dual-modality positron emission tomography/computed tomography imaging. *Invest Radiol.* 2003;38:784–789.
13. Dizendorf EV, Treyer V, von Schulthess GK, Hany TF. Application of oral contrast media in coregistered positron emission tomography-CT. *AJR.* 2002;179:477–481.
14. Dizendorf E, Hany TF, Buck A, von Schulthess GK, Burger C. Cause and magnitude of the error induced by oral CT contrast agent in CT-based attenuation correction of PET emission studies. *J Nucl Med.* 2003;44:732–738.
15. Cohade C, Osman M, Nakamoto Y, et al. Initial experience with oral contrast in PET/CT: phantom and clinical studies. *J Nucl Med.* 2003;44:412–416.
16. Berthelsen AK, Holm S, Loft A, Klausen TL, Andersen F, Højgaard L. PET/CT with intravenous contrast can be used for PET attenuation correction in cancer patients. *Eur J Nucl Med Mol Imaging.* 2005;32:1167–1175.
17. Yau Y, Chan W, Tam Y, et al. Application of intravenous contrast in PET/CT: does it really introduce significant attenuation correction error? *J Nucl Med.* 2005;46:283–291.
18. Nehmeh SA, Erdi YE, Kalagian H, et al. Correction for oral contrast artifacts in CT attenuation-corrected PET images obtained by combined PET/CT. *J Nucl Med.* 2003;44:1940–1944.